Title
Functional prokaryotic–eukaryotic chimera from the pentameric ligand-gated ion channel family

Journal
Proceedings of the National Academy of Sciences of the United States of America, 108(29)

ISSN
0027-8424

Authors
Duret, Guillaume
Van Renterghem, Catherine
Weng, Yun
et al.

Publication Date
2011-07-19

DOI
10.1073/pnas.1104494108

Peer reviewed

Functional prokaryotic–eukaryotic chimera from the pentameric ligand-gated ion channel family

Guillaume Duret[a,b], Catherine Van Renterghem[a,b], Yun Weng[c], Marie Prevost[a,b], Gustavo Moraga-Cid[a,b], Christèle Huon[a,b], James M. Sonner[c], and Pierre-Jean Corringer[a,b,1]

[a]Institut Pasteur, Groupe Récepteurs-Canaux, F-75015 Paris, France; [b]Centre National de la Recherche Scientifique, Unité de Recherche Associée 2182, F-75015 Paris, France; and [c]Department of Anesthesia and Perioperative Care, University of California, San Francisco, CA 94143

Edited* by Jean-Pierre Changeux, Institut Pasteur, Paris Cedex 15, France, and approved June 3, 2011 (received for review March 30, 2011)

Pentameric ligand-gated ion channels (pLGICs), which mediate chemo-electric signal transduction in animals, have been recently found in bacteria. Despite clear sequence and 3D structure homology, the phylogenetic distance between prokaryotic and eukaryotic homologs suggests significant structural divergences, especially at the interface between the extracellular (ECD) and the transmembrane (TMD) domains. To challenge this possibility, we constructed a chimera in which the ECD of the bacterial protein GLIC is fused to the TMD of the human α1 glycine receptor (α1GlyR). Electrophysiology in *Xenopus* oocytes shows that it functions as a proton-gated ion channel, thereby locating the proton activation site(s) of GLIC in its ECD. Patch-clamp experiments in BHK cells show that the ion channel displays an anionic selectivity with a unitary conductance identical to that of the α1GlyR. In addition, pharmacological investigations result in transmembrane allosteric modulation similar to the one observed on α1GlyR. Indeed, the clinically active drugs propofol, four volatile general anesthetics, alcohols, and ivermectin all potentiate the chimera while they inhibit GLIC. Collectively, this work shows the compatibility between GLIC and α1GlyR domains and points to conservation of the ion channel and transmembrane allosteric regulatory sites in the chimera. This provides evidence that GLIC and α1GlyR share a highly homologous 3D structure. GLIC is thus a relevant model of eukaryotic pLGICs, at least from the anionic type. In addition, the chimera is a good candidate for mass production in *Escherichia coli*, opening the way for investigations of "druggable" eukaryotic allosteric sites by X-ray crystallography.

Gloeobacter violaceus | allosteric effector | evolution | fusion protein | membrane protein

Pentameric ligand-gated ion channels (pLGICs) mediate chemo-electric signal transduction in animals, thereby fulfilling key physiological functions, including neurotransmission. They are composed of five identical or homologous subunits and carry one to five agonist binding sites on their extracellular domain (ECD) that govern the opening/closing motion of the ion channel within the transmembrane domain (TMD, composed of four helices labeled M1–M4). In human, ≈40 genes code for pLGIC subunits that are organized into two phylogenetic subclasses: cationic excitatory channels, such as nicotinic acetylcholine (nAChR) and $5HT_3$ receptors, and anionic inhibitory channels, such as glycine and $GABA_A$ receptors (1). More recently, several new members of the family have been discovered in prokaryotes (2), such as the homologous protein from *Gloeobacter violaceus* (GLIC), which forms a homopentamer functioning as a proton-gated ion channel (3).

Eukaryotic and prokaryotic receptors clearly display homologous structures, characterized by a highly conserved β-sandwich-folded ECD coupled to an all-helix TMD, as described by electron microscopy observation of the *Torpedo* nAChR (TnAChR) (4), and the X-ray structures of the acetylcholine binding protein (AChBP) (5), of the prokaryotic homologs ELIC (6) and GLIC (7, 8), and of the GluCl receptor from *Caenorhabditis elegans* (9). However, important local differences exist between the GLIC/ELIC/GluCl X-ray and the TnAChR electron microscopy structures, especially regarding loops at the ECD–TMD interface and the vertical register of the TMD helices. These discrepancies might be due to the medium resolution of electron microscopy data but can also come from the phylogenetic distances between these homologs. In the study reported here we challenged the structural and functional compatibility between the ECD of the prokaryotic GLIC and the TMD of the eukaryotic α1GlyR and constructed a prokaryotic–eukaryotic chimera composed of these two domains.

Results

Design of a $GLIC_{ECD}$-$α1GlyR_{TMD}$ Chimera Minimizing Structural Mismatches. We aligned the GLIC sequence with two representative homomeric members of the family, anionic α1GlyR and cationic α7nAChR (Fig. S1). For the ECD, this alignment shows sequence identity of 18–19% between GLIC and both α7nAChR and α1GlyR. In contrast, for the TMD, sequence identity is 20% and 26% between GLIC and α7nAChR and α1GlyR, respectively. The higher score for GLIC/α1GlyR alignment is in line with the conservation of clusters of residues all along the sequence of the TMD, whereas the alignment between GLIC and α7nAChR for the M3 and M4 segments remains ambiguous (10, 11). Consequently, we selected the α1GlyR for the construction of the chimera.

Together with the alignment, the X-ray structure of GLIC allows for several predictions that help the construction of a chimera with minimum putative mismatches at the prokaryotic–eukaryotic protein interface (Fig. 1). (*i*) The point of fusion was selected at the site of the conserved RQ (192–193) motif that precedes M1. (*ii*) The tip of loop 7 of the ECD protrudes down into the TMD, at the level of which the YPF (119–121) motif elicits multiple interactions. Consequently, it was mutated into the FPM sequence of the α1GlyR. (*iii*) Because the C-terminal tip of M4 also elicits several contact points with loop 7 of the ECD, this portion was mutated into that of GLIC [FGF (315–317)]. (*iv*) The large cytoplasmic loop, which is absent in GLIC and removable in eukaryotic pLGIC (12), was replaced by the short segment of GLIC [SQP (283–285)].

$GLIC_{ECD}$-$α1GlyR_{TMD}$ Forms a Proton-Gated Channel. Two-electrode voltage-clamp electrophysiology on *Xenopus* oocytes expressing the chimera shows that it forms a proton-activated channel (Fig. 2). The activation shows a relatively fast kinetic, and the current reaches a plateau or displays a slow decay during prolonged application at the highest proton concentrations (see pH 5 in Fig. 2*A*). At pH 5, the current decay was fitted to a single exponential with an average rate constant of 0.029 ± 0.016 s^{-1} (i.e., a time

Author contributions: G.D., C.V.R., Y.W., J.M.S., and P.-J.C. designed research; G.D., C.V.R., Y.W., and C.H. performed research; G.D., C.V.R., Y.W., M.P., G.M.-C., J.M.S., and P.-J.C. analyzed data; and G.D., C.V.R., M.P., G.M.-C., J.M.S., and P.-J.C. wrote the paper.

The authors declare no conflict of interest.

*This Direct Submission article had a prearranged editor.

[1]To whom correspondence should be addressed. E-mail: pjcorrin@pasteur.fr.

This article contains supporting information online at www.pnas.org/lookup/suppl/doi:10.1073/pnas.1104494108/-/DCSupplemental.

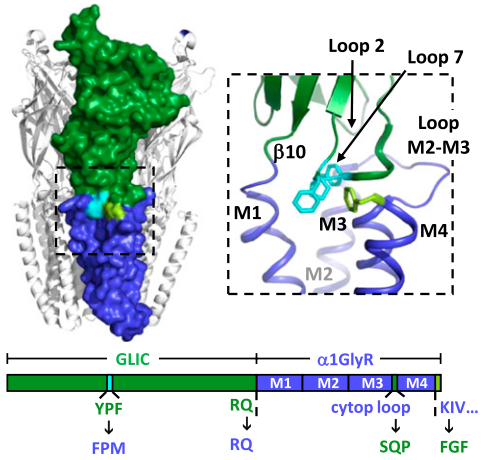

Fig. 1. $GLIC_{ECD}$-$α1GlyR_{TMD}$ chimera. (*Upper*) Representation of the chimera based on the GLIC structure. The ECD (green) is from GLIC and the TMD (blue) from α1GlyR. (*Lower*) Linear sequence with local modifications performed at the ECD–TMD interface and on the cytoplasmic domain (see text).

constant of 42 ± 18 s; $n = 65$). The EC_{50} of the maximal response to protons is 3.3 ± 0.1 × 10^{-7} M (pH 6.5) with a Hill coefficient nH = 1.10 ± 0.05. This activated current is fully inhibited by picrotoxinin, which is a potent inhibitor of both GLIC and α1GlyR. At pH 5.5, the application of 10 and 50 μM picrotoxinin yielded a 55% ± 11% and 93% ± 6% inhibition, respectively ($n = 3$; Fig. 2*C*). In addition, the application of picrotoxinin at pH 8 produces a significant decrease of the holding current at −60 mV, suggesting a slight activation at pH 8. Activation at higher proton concentrations produced currents of identical amplitude to that observed at pH 5, indicating that the plateau for activation has been reached.

$GLIC_{ECD}$-$α1GlyR_{TMD}$ Carries an Intact Anionic Channel in Whole-Cell and Single-Channel Recordings. Current-voltage (I-V) relationships in oocytes (Fig. 2*D*) show that the current elicited by proton concentrations between 10^{-8} and 10^{-5} M is characterized by a marked outward rectification. The variation of the E_{rev} as a function of external NaCl concentration is well fitted by the Goldman-Hodgkin-Katz equation assuming that only chloride ions contribute to the currents (Fig. 2*E*).

Outside-out patch-clamp recordings from BHK cells expressing the chimera showed single-channel activity when switching the extracellular pH from 8 to 6 (Fig. 3*A*). Such events were not detected in patches excised from BHK cells transfected with GFP only. In our recording conditions, the open state probability was close to zero at pH 8, in patches producing an activity at pH 6.

Single-channel currents elicited at pH 6 were undetectable at 0 mV in symmetrical chloride conditions (Fig. 3*B*), whereas inward currents could be detected at up to +20 mV on the same patch when the extracellular chloride concentration was reduced to one third. Thus, single-channel current polarity varies with the reversal potential for chloride ions, confirming that the chimera is selective for anions. Single-channel recordings performed at various stationary holding voltages (Fig. 3*C*) result in a linear I-V relationship with a conductance of 85 pS between −80 and −30 mV (Fig. 3*C*). For direct comparison, we challenged the hα1GlyR and GLIC T255A [selected because it is significantly activated at pH 6 (13)]. pH 6-elicited currents through GLIC T255A channel indicates a single-channel conductance of 8 pS between −80 and 0 mV, in agreement with Bocquet et al. (3). Glycine (50 mM)-elicited currents on the hα1GlyR indicate a single-channel conductance of 85 pS (Fig. 3*C* and Fig. S2). Therefore, the chimera exhibits a single-channel conductance value identical to that of the α1GlyR channel.

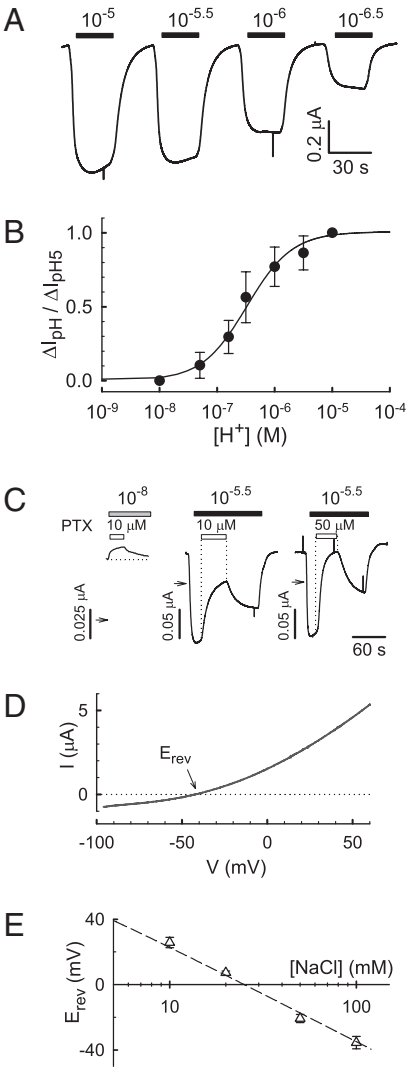

Fig. 2. Electrophysiological characteristics of the $GLIC_{ECD}$-$α1GlyR_{TMD}$ chimera expressed in oocytes. (*A*) Representative trace of the current when the extracellular proton concentration is changed from 10^{-8} M to the indicated concentration (10^{-pH} M). All recordings are performed at −60 mV unless otherwise specified. (*B*) Proton dose–response curve reporting the peak current at each proton concentration, normalized to the peak current at pH 5. Fit to the Hill equation yields EC_{50} = 3.3 (± 0.1) × 10^{-7} M (= pH 6.5) and nH = 1.10 ± 0.05 (n = 144 oocytes; values ± SD). (*C*) Inhibition of proton-elicited current by picrotoxinin (PTX). Arrow indicates the peak current value at pH 6.8. (*D*) Representative I-V curve obtained from voltage-ramps (0.25 V/s) representing current values activated at pH 6.8 minus the current background at pH 8. (*E*) E_{rev} measured at different external NaCl concentrations. The decreased E_{rev} as the ionic concentration increases demonstrates that the channel is selective for anions. Each point results from at least three independent experiments. For all plots, error bars report SD.

Glycine receptor channels, including the α1GlyR, are known to exhibit several conductance sublevels in addition to the major 85-pS large conductance level recorded above (14). Current traces from the chimera show additional lower amplitude single-channel events (Fig. S2*B*), which may correspond respectively to substates III, IV, V, and VI, in addition to the main state II detected by Borman et al. (Fig. 3 of ref. 14). These results suggest that the subconductance levels are also preserved in the chimera.

$GLIC_{ECD}$-$α1GlyR_{TMD}$ Is Potentiated by General Anesthetics, Alcohols, and Ivermectin. GLIC and α1GlyR display opposite pharmacological properties regarding most allosteric modulators. GLIC is

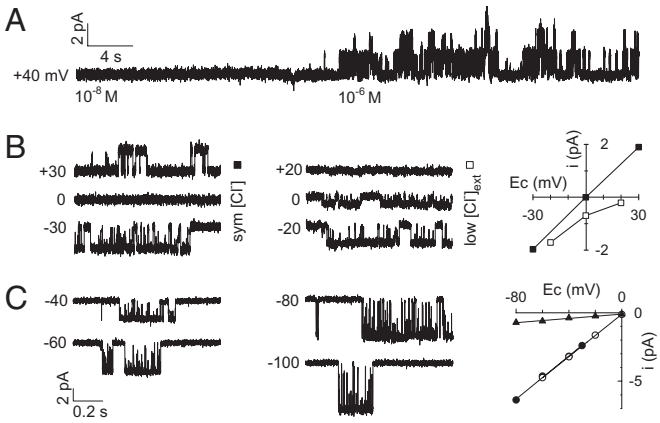

Fig. 3. Outside-out patches from cells expressing the $GLIC_{ECD}$-α1$GlyR_{TMD}$ chimera. (*A*) Activation of single-channel activity by increasing the extracellular proton concentration from 10^{-8} to 10^{-6} M. The N.Po parameter (number of channels active in the patch × mean single-channel open-state probability) is 0 at pH 8 and 0.47 at pH 6. (*B*) Anion selectivity of the channel inferred from single-channel recording in symmetrical chloride conditions and low (one-third) external chloride conditions (see text). (*C*) Currents measured on patches from cells expressing $GLIC_{ECD}$-α1$GlyR_{TMD}$ (10^{-6} M proton) and I-V plot for $GLIC_{ECD}$-α1$GlyR_{TMD}$ (filled circles), α1GlyR (50μM glycine, open circles), and GLIC (10^{-6} M proton, filled triangles). Linear fits of the data (Fig. S2) give single-channel conductances of 85, 85, and 8.5 pS, respectively.

inhibited by a wide range of general anesthetics, including volatile and injected compounds at clinical concentrations (13, 15). It is also inhibited by alcohols ranging from propanol to decanol, whereas methanol and ethanol have a weak potentiating effect (16), and is weakly inhibited by the antiparasitic compound ivermectin (18.8% ± 2.1% at 30 μM, $n = 3$). In contrast, α1GlyR is potentiated by volatile (17) and injected anesthetics such as propofol (18). It is potentiated by alcohols including long-chain alcohols (19), as well as ivermectin (20).

The sensitivity of the chimera toward these effectors was investigated at 10^{-8} M and $10^{-6.8}$ M (EC_{30}) proton concentrations. All tested general anesthetics robustly potentiate the chimera (Fig. 4). The most potent general anesthetic is propofol, which triggers an up to 10-fold potentiation of the pH 6.8-elicited currents with an EC_{50} of 340 ± 90 μM (nH = 1.45 ± 0.37). Although it takes some time to fully wash away, the effect of propofol is reversible. Robust propofol-elicited currents are also observed at pH 8 (Fig. 4 *A* and *C*, *Insert*). However, we cannot conclude a direct activation here because 10^{-8} M of proton possibly produces a minor activation (Fig. 2*C*). However, direct activation would be reminiscent of homomeric α1GlyR and α1β2γ2-$GABA_A$ receptor that are activated by volatile general anesthetics and hexanol in the absence of agonist (Fig. S3).

Unexpectedly, the time course of the propofol response is biphasic, the rapid and transient potentiation being followed by an exponential decay of the response (Fig. S4). In addition, upon removal of propofol, a rebound current (i.e., a transient increase in currents) is observed (asterisk in Fig. 4*A*). These observations suggest that propofol promotes desensitization and/or an additional allosteric inhibition of the chimera. Such decay is also observed for other potentiators described below (isoflurane in Fig. 4*B* and hexanol in Fig. 5*A*).

All tested volatile anesthetics potentiate the chimera as well, although less potently than propofol, at pH 6.8 (Fig. 4*B*) and pH 8 (Fig. S5). The maximum potentiation at pH 6.8 could not be determined owing to the limitation in anesthetics' solubility. The concentrations reuired for a 200% potentiation of the pH 6.8-elicited currents are 0.55, 1.04, 1.05, and 4.15 mM for halothane,

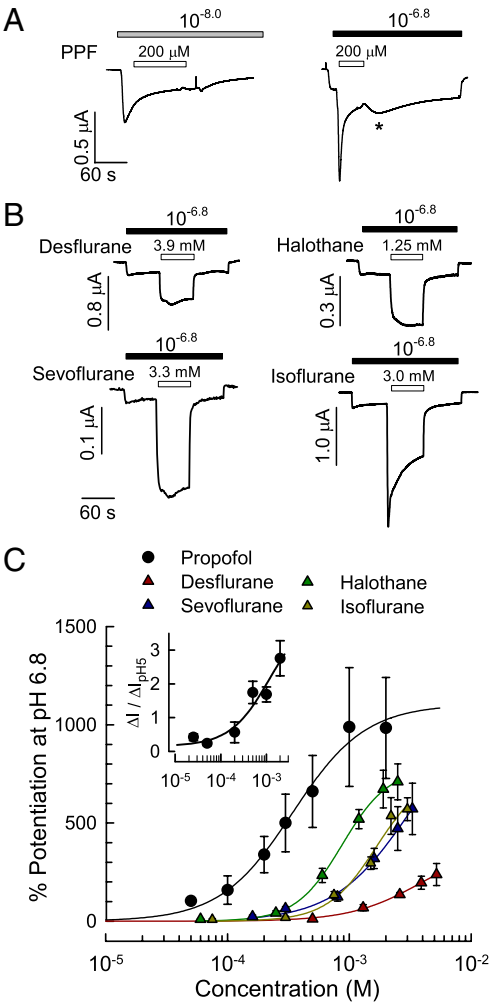

Fig. 4. General anesthetics potentiate $GLIC_{ECD}$-α1$GlyR_{TMD}$. (*A*) Representative current traces in the presence of proton (upper bar giving concentration) and propofol (PPF, lower bar). The current rebound when PPF is rinsed (*) is repeatedly observed. (*B*) Similar experiments with four volatile anesthetics. (*C*) Dose–response curve for the potentiation by general anesthetics at pH 6.8. The fit of the propofol dose–response curve to the Hill equation estimated an EC_{50} of 340 ± 90 μM. Higher concentrations could not be tested owing to the solubility limit. *Insert:* Activation by PPF at pH 8 normalized to the maximal current measured at pH 5. $n = 3$ independent oocytes for each concentration of each compound; values ± SD.

isoflurane, sevoflurane, and desflurane, respectively, compared with the 0.12 mM required for a 200% potentiation by propofol.

Ethanol and the long-chain alcohol hexanol were also found to promote reversible potentiation of the chimera (Fig. 4). A high concentration of ethanol is necessary (>200 mM) to potentiate pH 6.8-elicited currents. Hexanol is more potent and promotes up to eightfold potentiation at 30 mM. Hexanol also activates/potentiates currents at pH 8 at higher concentrations. Finally, we found that ivermectin potentiates the chimera. This potentiation is transient and followed by a slow, complete, and irreversible decay of the response (Fig. 5 and Fig. S4). A 200% potentiation can be observed in the presence of 0.9 μM ivermectin and is followed by an inhibition with a decay constant of 0.02 s^{-1}.

Discussion

$GLIC_{ECD}$-α1$GlyR_{TMD}$ Chimera Is a Proton-Activated Chloride Channel. A distinctive feature of the chimera is that it is activated by protons, whereas the α1GlyR is inhibited by protons in a noncompetitive manner (21). This shows that the proton sensor of

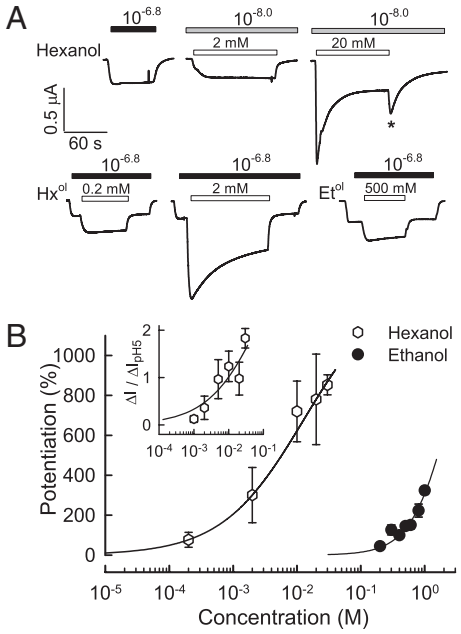

Fig. 5. Alcohols potentiate $GLIC_{ECD}$-$\alpha1GlyR_{TMD}$. (*A*) Representative current traces in the presence of protons (*Upper*) and hexanol or ethanol (Hx^{ol} or Et^{ol}, *Lower*). Upon rinsing, a rebound current is measured for high hexanol concentrations (*). (*B*) Dose–response curve for the potentiation by alcohols at pH 6.8. Higher concentrations could not be tested owing to the solubility limit or some irreversible effect on oocytes. (*Inset*) Activation by hexanol at pH 8 normalized to the maximal current measured at pH 5. $n = 3$ for each concentration.

GLIC is carried by the ECD. The chimera shows a time course of proton-elicited activation and decay similar to that of GLIC. However, distinctively from GLIC, which is activated at a pH below 6 ($pH_{50} = 5$), the chimera is already activated at pH 7 ($pH_{50} = 6.5$). This suggests that the chimera is allosterically stabilized in the active conformation compared with GLIC. Similar phenotypes are obtained on GLIC with a single mutation at position 9′ within the channel (3) or T255A within the general anesthetics' binding site (13).

Whole-cell and single-channel recordings demonstrate that the chimera carries a chloride-selective channel with a unitary conductance equal to that of the intact α1GlyR. Furthermore, conductance sublevels similar to the ones observed on α1GlyR are detected on the chimera. The removal of the intracellular loop region, and more importantly coupling of the α1GlyR TMD with the ECD of GLIC, preserves intact ion channel properties.

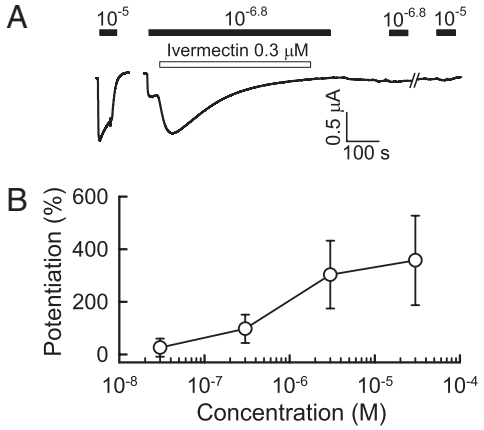

Fig. 6. Ivermectin has an irreversible effect on $GLIC_{ECD}$-$\alpha1GlyR_{TMD}$. (*A*) Representative current traces in the presence of protons (*Upper*) and ivermectin (*Lower*). The inhibitory effect after prolonged exposure irreversibly prevents further activation, as shown by the postapplications of protons. (*B*) Dose–response curve for the potentiation by ivermectin at pH 6.8. Higher concentrations could not be tested owing to the solubility limit.

$GLIC_{ECD}$-$\alpha1GlyR_{TMD}$ Chimera Displays Typical α1GlyR Transmembrane Pharmacology. All effectors tested on the chimera, except ethanol, display opposite pharmacological effects by inhibiting GLIC and potentiating the α1GlyR. We show here that they all potentiate the proton-elicited currents of the chimera. Propofol, ethanol, hexanol, and ivermectin potentiations of the chimera occur in the same concentration ranges as what has been published for the α1GlyR (18–20). Notably, the long-chained alcohols are more effective at lower concentrations than short-chained alcohols, and high-ethanol concentrations (>50 mM) are required to potentiate both the α1GlyR and the chimera. The volatile anesthetics seem to be slightly less effective than what is reported on the α1GlyR (22, 23). Ivermectin potentiates the α1GlyR at concentrations below 0.03 μM and activates it at concentrations above 0.03 μM, involving a complex mechanism that is largely irreversible.

Overall, despite the absence of the α1GlyR large cytoplasmic loop, which contributes to high-affinity ethanol and propofol modulation (24) and the different ECD, the pharmacologies of potentiation observed on the α1GlyR and the chimera are similar. This supports a location of the main binding sites for allosteric modulation within the TMD. This idea is already supported by numerous mutational (25) and affinity labeling (26) analyses performed on the glycine/$GABA_A$ receptors (27) and by the recent X-ray crystallographic data on GLIC (28). These studies stress the contribution of two cavities in the allosteric modulation, both located in the upper part of the TMD: one at the center of the four helices bundle in each subunit, and one at the interface between subunits. In the chimera, only residues from the α1GlyR border these cavities that seem to be unaltered in the chimeric context.

Interestingly, most allosteric potentiators tested produced a biphasic effect: a rapid potentiation of pH-evoked currents, followed by a slow decrease of the currents that sometimes reaches intensities lower than that of the control response to proton. This indicates that most effectors either promote receptor desensitization (i.e., a slow isomerization of the protein toward a closed conformation refractory to activation) or slowly bind to an additional inhibitory site. It is noteworthy that the proton-elicited currents show a similar phenomenon, as observed at pH 5 on the trace in Fig. 2, where the peak current is followed by a slow decrease of the response. The fact that such a decrease is promoted by effectors as diverse as protons, volatile general anesthetics, propofol, and hexanol argues in favor of a mechanism intrinsic to the receptor, most likely a desensitization process. Such a desensitization-driven effect has been described for $GABA_A$ receptors (29) and for the α1GlyR (30) with alcohols. However, we often observed with hexanol and propofol a repotentiation upon rinsing (rebound current; see asterisk on traces in Figs. 4 and 5). This effect might reflect the presence of additional inhibitory binding sites displaying a faster dissociation constant than the activation sites.

Functional Data Support a Structural Intactness of the $\alpha1GlyR_{TMD}$ Structure When Coupled to $GLIC_{ECD}$. Regarding the ECD portion, atomic resolution data of eukaryotic pLGICs have been obtained thanks to AChBP. The β-sandwich core of AChBP can be almost perfectly superimposed to the β-sandwich core of both GLIC and ELIC, whereas most peripheral loop regions are structurally variable owing to local flexibility and sequence divergence. The main exception concerns loops 2 and 7. The X-ray structure of GLIC's isolated ECD shows that these loops adopt a disordered

conformation in the absence of the TMD (28), whereas they are well structured in the full protein.

Regarding the TMD, comparison of GLIC and TnAChR shows the conservation of the organization of the α-helices bundle. M2 borders the channel and is surrounded by M1 and M3, whereas M4 is peripheral. The axis and position of all helices are well conserved, but important discrepancies exist between the registers of the M2 helices. For instance, residues in position E-2′ of GLIC align with residues T2′ in TnAChR. Additionally, all helices are extended by one additional turn in TnAChR compared with GLIC. The loop linking the M2 and M3 segments (M2–M3 loop) is located within the subunit in TnAChR but at the interface between subunits in GLIC. SCAM (substituted cysteine accessibility method) studies on $GABA_A$ receptors tend to favor the TnAChR model in the upper part of the channel (31). Cysteine cross-linking experiments investigating the register of M2 and M3 helices support the TnAChR model in one study (32) and the GLIC model in another (33). In addition, no satisfactory alignment can be proposed regarding the C-terminal portion of the TMD (including M2–M3 loop, M3, and M4 segments) between anionic and cationic homologs. This further stresses that homology models of anionic homologs based on TnAChR have to be used cautiously.

Our observations provide strong evidence that the structure of the TMD of α1GlyR is unchanged when incorporated into the chimera. (*i*) The pore of the chimera displays an ionic selectivity, a single-channel conductance, and even conductance sublevels close, if not identical, to those of the α1GlyR. This reveals a preserved structure of the bundle of M2 helices lining the pore. (*ii*) The chimera displays a pharmacology for eight different allosteric modulators typical of the α1GlyR, pointing to an overall conservation of the corresponding binding sites. This supports a structural intactness of the TMD and notably of the upper part that carries the binding sites of general anesthetics and alcohols (13, 25, 26). (*iii*) The sequences of GLIC and α1GlyR display clear homology all along the TMD. Altogether, we provide evidence that GLIC and α1GlyR share highly homologous 3D structures, supporting that GLIC is a relevant model for investigating both structure and gating of eukaryotic receptors from the anionic family. This idea is further supported by the recent X-ray structure of the GluCl receptor from *Caenorhabditis elegans*, which is clearly homologous to the structures of both GLIC and ELIC (9).

Common Gating Mechanism Within the Whole pLGIC Superfamily. A striking conclusion of the present study is that, despite billions of years of evolution, the ECD and the TMD are still compatible to yield a functional ligand-gated ion channel. This implies the conservation of key motifs required for the conformational transition to be transmitted between the ECD and the TMD: the pre-M1, loop2, and loop7 from the TMD, with the top of each helix and loop M2–M3 from the TMD. The structure of GLIC shows that the interactions occurring at the domains interface (TMD–ECD) are, for the most part, intrasubunit interactions, with loop 7 having the central role of interacting directly with all other motifs (Fig. 1 and Fig. S6). The exception to that observation is the interaction between loop M2–M3 of one subunit with the top of M1 from the adjacent subunit.

Altogether, the gating mechanism seems to be conserved within the whole family, because functional cationic/cationic chimera between α7nAChR (ECD) and $5HT_3R$ (TMD) (34) and cationic/anionic chimera between α7nAChR (ECD) and α1GlyR (TMD) (35) have also been described. Sequence comparison of representative members of the family shows that only a few residues are universally conserved in the coupling region (Fig. S6). (*i*) Three titrable residues that are interacting in the GLIC structure, D32, R192, and D122. The two earlier residues correspond to E42 and R209 in α1nAChR and form a salt bridge required for proper folding (36). (*ii*) A cluster of hydrophobic residues from loop 7 that mainly contribute to interaction with the TMD. (*iii*) Two canonical proline residues within loop 7 and loop M2–M3, which in GLIC seem required for the loop conformation. Most of these residues seem essential for proper folding of the subunit. It can thus be speculated that gating is the result of shape complementarity between surfaces of the ECD and the TMD, rather than specific amino acid interactions. Accordingly, the amino acid sequence disparities at this level would be involved in fine tuning of the gating, for instance by modulating the kinetics of activation as shown for α7nAChR-α1GlyR chimera (35).

It is worth emphasizing that the present chimera was designed with few modifications at the ECD–TMD interface and readily produced a functional channel. To minimize putative mismatches at the ECD–TMD interface, the tip of the loop 7 was mutated into the tip of α1GlyR (Y119F/F121M) and the C-terminal extracellular tail to the C_{ter} sequence of GLIC (K^{315}IVRREDVHNQ into F^{315}GF). The effects of both sets of mutations were investigated by performing the reversed mutations independently on the chimera (Fig. S7). Interestingly, both sets of reversed mutations produce a similar phenotype, characterized by much faster apparent rates of activation, followed by a rapid decay of the response to reach eventually a plateau. The dose–response curves as well as the maximal proton-elicited currents are not significantly different from that of the parent chimera. These data suggest that both mutations individually accelerate the kinetics of the channel, with the appearance of a fast desensitization component. Altogether these data illustrate the robustness of the coupling between the ECD and the TMD and highlight the key contribution of variable residues between GLIC and the α1GlyR in modulating the kinetics of the channel.

Conclusion

Structural studies of neurotransmitter receptors from the pLGIC superfamily have been undermined by the difficulty to purify and crystallize eukaryotic membrane proteins. The $GLIC_{ECD}$-$\alpha1GlyR_{TMD}$ chimera does not require the posttranslational modifications that the eukaryotic ECD typically undergoes. It is therefore a good candidate for expression in *Escherichia coli* and subsequent X-ray crystallography. Our work opens the way to atomic-resolution structural investigations of the eukaryotic TMD, which includes the ion channel and bears "druggable" regulatory binding sites that are clinically relevant.

Materials and Methods

The cDNA of the chimera was constructed as a synthetic gene (Geneart), fused at the 5′ end with the coding sequence for eukaryotic signal peptide and at the 3′ end to an HA tag coding region, and was cloned in the pMT3 vector as previously described (3). Two-electrode voltage clamp electrophysiology in *Xenopus* oocytes was performed as previously described (13). Patch-clamp recordings were performed on the tk-ts13 variant of BHK cells transfected using the calcium phosphate procedure. Single-channel currents from outside-out patches were low-pass filtered at 1–3 kHz (chimera and α1GlyR) or 0.3 kHz (GLIC). The signal was digitized at a sampling frequency of 10–40 kHz. The intracellular solution was composed of 130 mM CsCl, 1 mM $MgCl_2$, 10 mM 2-(*N*-morpholino)ethanesulfonic acid (MES), and 10 mM 1,2-bis(o-aminophenoxy)ethane-*N*,*N*,*N*′,*N*′-tetraacetic acid (BAPTA), adjusted to pH 7.2 with *N*-methyl-D-glucamine. In symmetrical conditions, the extracellular solution was composed of 150 mM NaCl, 1 mM $MgCl_2$, 1 mM $CaCl_2$, and 10 mM Mes, adjusted to the desired pH. In the low extracellular chloride solution, two-thirds of NaCl was replaced by sodium gluconate, moving E_{Cl} to +35 mV (pH 8) or +30 mV (pH 6). Specifications are provided in *SI Materials and Methods*.

ACKNOWLEDGMENTS. We thank Jean-Pierre Changeux for useful comments. This work was supported by the region Ile de France [Neuropole de Recherche Francilien (NERF) program to G.D.], the Commission of the European Communities (Neurocypres project), and the Louis D. Foundation from the Institut de France.

1. Le Novère N, Corringer PJ, Changeux JP (1999) Improved secondary structure predictions for a nicotinic receptor subunit: Incorporation of solvent accessibility and experimental data into a two-dimensional representation. *Biophys J* 76: 2329–2345.
2. Tasneem A, Iyer LM, Jakobsson E, Aravind L (2005) Identification of the prokaryotic ligand-gated ion channels and their implications for the mechanisms and origins of animal Cys-loop ion channels. *Genome Biol* 6:R4.
3. Bocquet N, et al. (2007) A prokaryotic proton-gated ion channel from the nicotinic acetylcholine receptor family. *Nature* 445:116–119.
4. Unwin N (2005) Refined structure of the nicotinic acetylcholine receptor at 4A resolution. *J Mol Biol* 346:967–989.
5. Brejc K, et al. (2001) Crystal structure of an ACh-binding protein reveals the ligand-binding domain of nicotinic receptors. *Nature* 411:269–276.
6. Hilf RJC, Dutzler R (2008) X-ray structure of a prokaryotic pentameric ligand-gated ion channel. *Nature* 452:375–379.
7. Bocquet N, et al. (2009) X-ray structure of a pentameric ligand-gated ion channel in an apparently open conformation. *Nature* 457:111–114.
8. Hilf RJC, Dutzler R (2009) Structure of a potentially open state of a proton-activated pentameric ligand-gated ion channel. *Nature* 457:115–118.
9. Hibbs RE, Gouaux E (2011) Principles of activation and permeation in an anion-selective Cys-loop receptor. *Nature* 474:53–60.
10. Baenziger JE, Corringer P-J (2011) 3D structure and allosteric modulation of the transmembrane domain of pentameric ligand-gated ion channels. *Neuropharmacology* 60:116–125.
11. Bertaccini EJ, Wallner B, Trudell JR, Lindahl E (2010) Modeling anesthetic binding sites within the glycine alpha one receptor based on prokaryotic ion channel templates: The problem with TM4. *J Chem Inf Model* 50:2248–2255.
12. Jansen M, Bali M, Akabas MH (2008) Modular design of Cys-loop ligand-gated ion channels: Functional 5-HT3 and GABA rho1 receptors lacking the large cytoplasmic M3M4 loop. *J Gen Physiol* 131:137–146.
13. Nury H, et al. (2011) X-ray structures of general anaesthetics bound to a pentameric ligand-gated ion channel. *Nature* 469:428–431.
14. Bormann J, Rundström N, Betz H, Langosch D (1993) Residues within transmembrane segment M2 determine chloride conductance of glycine receptor homo- and hetero-oligomers. *EMBO J* 12:3729–3737.
15. Weng Y, Yang L, Corringer PJ, Sonner JM (2010) Anesthetic sensitivity of the Gloeobacter violaceus proton-gated ion channel. *Anesth Analg* 110:59–63.
16. Howard RJ, et al. (2011) Structural basis for alcohol modulation of a pentameric ligand-gated ion channel. *Proc Natl Acad Sci USA* 108:12149–12154.
17. Beckstead MJ, Phelan R, Mihic SJ (2001) Antagonism of inhalant and volatile anesthetic enhancement of glycine receptor function. *J Biol Chem* 276:24959–24964.
18. O'Shea SM, Becker L, Weiher H, Betz H, Laube B (2004) Propofol restores the function of "hyperekplexic" mutant glycine receptors in *Xenopus* oocytes and mice. *J Neurosci* 24:2322–2327.
19. Wick MJ, et al. (1998) Mutations of gamma-aminobutyric acid and glycine receptors change alcohol cutoff: Evidence for an alcohol receptor? *Proc Natl Acad Sci USA* 95: 6504–6509.
20. Shan Q, Haddrill JL, Lynch JW (2001) Ivermectin, an unconventional agonist of the glycine receptor chloride channel. *J Biol Chem* 276:12556–12564.
21. Chen Z, Dillon GH, Huang R (2004) Molecular determinants of proton modulation of glycine receptors. *J Biol Chem* 279:876–883.
22. Lobo IA, Harris RA (2005) Sites of alcohol and volatile anesthetic action on glycine receptors. *Int Rev Neurobiol* 65:53–87.
23. Dupre ML, Broyles JM, Mihic SJ (2007) Effects of a mutation in the TM2-TM3 linker region of the glycine receptor alpha1 subunit on gating and allosteric modulation. *Brain Res* 1152:1–9.
24. Moraga-Cid G, Yevenes GE, Schmalzing G, Peoples RW, Aguayo LG (2011) A single phenylalanine residue in the main intracellular loop of [alpha]1 [gamma]-aminobutyric acid type A and glycine receptors influences their sensitivity to propofol. *Anesthesiology*, 10.1097/ALN.0b013e31822550f7.
25. Mihic SJ, et al. (1997) Sites of alcohol and volatile anaesthetic action on GABA(A) and glycine receptors. *Nature* 389:385–389.
26. Li GD, et al. (2006) Identification of a GABAA receptor anesthetic binding site at subunit interfaces by photolabeling with an etomidate analog. *J Neurosci* 26: 11599–11605.
27. Franks NP (2008) General anaesthesia: From molecular targets to neuronal pathways of sleep and arousal. *Nat Rev Neurosci* 9:370–386.
28. Nury H, et al. (2010) Crystal structure of the extracellular domain of a bacterial ligand-gated ion channel. *J Mol Biol* 395:1114–1127.
29. Dopico AM, Lovinger DM (2009) Acute alcohol action and desensitization of ligand-gated ion channels. *Pharmacol Rev* 61:98–114.
30. Aguayo LG, Pancetti FC (1994) Ethanol modulation of the gamma-aminobutyric acidA- and glycine-activated Cl- current in cultured mouse neurons. *J Pharmacol Exp Ther* 270:61–69.
31. Wiltfong RE, Jansen M (2009) Probing protein packing surrounding the residues in and flanking the nicotinic acetylcholine receptor M2M3 loop. *J Neurosci* 29: 1626–1635.
32. Jansen M, Akabas MH (2006) State-dependent cross-linking of the M2 and M3 segments: Functional basis for the alignment of GABAA and acetylcholine receptor M3 segments. *J Neurosci* 26:4492–4499.
33. Lobo IA, Trudell JR, Harris RA (2004) Cross-linking of glycine receptor transmembrane segments two and three alters coupling of ligand binding with channel opening. *J Neurochem* 90:962–969.
34. Eiselé JL, et al. (1993) Chimaeric nicotinic-serotonergic receptor combines distinct ligand binding and channel specificities. *Nature* 366:479–483.
35. Grutter T, et al. (2005) A chimera encoding the fusion of an acetylcholine-binding protein to an ion channel is stabilized in a state close to the desensitized form of ligand-gated ion channels. *C R Biol* 328:223–234.
36. Lee WY, Sine SM (2005) Principal pathway coupling agonist binding to channel gating in nicotinic receptors. *Nature* 438:243–247.